Non-Reciprocal Acoustoelectric Amplification in Germanium-Based Lamb Wave Delay Lines

F. Hakim, M. Ramezani, S. Rassay, and R. Tabrizian
Department of Electrical and Computer Engineering, University of Florida, Gainesville, USA
email: hakimfaysal@ufl.edu

***Abstract*— This paper reports, for the first time, on the use of acoustoelectric effect in single crystal germanium (Ge) for non-reciprocal amplification of Lamb waves in radio frequency (RF) delay lines. Such delay lines enable realization of integrated full-duplex wireless front-end modules for emerging 5G applications. A thin aluminum nitride (AlN) piezoelectric film, with single-phase unidirectional transducers, is used to excite fundamental anti-symmetric (A_0) and symmetric (S_0) Lamb waves in Ge waveguide. The traveling waves are then amplified by application of a DC electric field across the Ge waveguide through the use of deformation-potential coupling between the traveling acoustic wave and DC-accelerated charge carriers. Mixed-domain analytical and numerical models are developed predicting 18-26 dB/mm amplification for S_0 and A_0 waves, respectively. Proof-of-concept delay lines are demonstrated operating at 72 MHz (A_0) and 250 MHz (S_0) frequencies showing transmission amplification of ~6 dB and ~8 dB upon application of 35 V and 40 V, respectively. Specifically, a non-reciprocal transmission ratio of 20 dB is measured for the S_0 wave, highlighting the potential of the germanium-based RF acoustic delay-lines for adoption in the forthcoming full-duplex front-end modules.**

I. Introduction

The new generation of wireless protocols (i.e. 5G and beyond) promise substantial enhancement in data-rate, band-width, and latency metrics by exploiting full-duplex communication schemes. Therefore, a recent wave of research, in various applied physics and engineering disciplines, has been focused on development of integrated non-reciprocal spectral processors that enable simultaneous data transmission and reception at the same time and within the same band. Non-reciprocal spectral processors have not been previously available in chip scale and the available macro-scale modules, such as ferrite-based isolators and circulators, where substantially handicapped for integration and frequency scaling. To replace these, a variety of integrated non-reciprocal components are recently introduced based on the use of time-variant systems [1,2], asymmetric physical nonlinearities [3], and directional polarization in mixed-domain systems [4-6]. Among these, DC-polarized non-reciprocal acoustic waveguides offer various advantages including large dynamic range of operation, extreme frequency scaling over the ultra- and super-high-frequency regimes, ultra-miniaturized form factors, and low insertion loss. These devices operate based on the use of acoustoelectric (AE) effect, commonly termed as 'wave-particle drag'. The AE effect occurs at the intersection of propagating acoustic waves / phonons and DC-accelerated charge carriers in piezoelectric semiconductors and enable energy exchange between mechanical and electronic domains [7]. The efficiency of such energy exchange depends on the piezoelectric coupling factor, which is responsible for generation of a traveling electric-field along with the acoustic wave, and the electron mobility, which defines the drift velocity of DC-accelerated electrons. Considering the very limited set of piezoelectric semiconductor materials that lack one or both of the above-mentioned merit figures, early demonstrations of the AE effects were not successful in realization of spectral processors with large non-reciprocal transduction ratio (NTR). Alternative solutions that are recently presented rely on wafer-level bonding of non-piezoelectric semiconductors on piezoelectric lithium niobate ($LiNbO_3$) substrates to amplify the piezoelectrically generated traveling electric-field at the interface of semiconductor and piezoelectric substrates. These heterogenous approaches suffer from wafer-level bonding challenges and do not offer a truly CMOS-integrated solution.

In this paper, we demonstrate the use of an entirely different physics for realization of non-reciprocal amplification in single crystal germanium (Ge). In this approach, the required electromechanical coupling is provided by the deformation-potential scattering that relates the electronic band-structure in semiconductors to lattice strain induced by the traveling acoustic wave. Benefitting from large deformation potential constant and high electron mobility, single crystal Ge enables a means for non-reciprocal acoustoelectric amplification that is only improving with the increase in operation frequency. Here, analytical and numerical models, along with Lamb-wave delay line test-vehicles, are presented to demonstrate the potential of single crystal Ge for realization of truly integrated non-reciprocal spectral processors for chip-scale full-duplex RF spectral processing.

II. Acoustoelectric Amplification in Ge

The multi-valley nature of conduction band in Ge makes phonon-electron interaction possible via deformation potential coupling. In this concept, an acoustic wave launched through a Ge waveguide modulates the electronic band structure along its propagation path and enforce re-distribution of free charge carriers with dynamics governed by inter-valley scattering principles. The anharmonicity of free carrier relaxation with acoustic wave propagation results in a non-zero-sum bunching of electrons behind or ahead of acoustic wave, which results in acoustoelectric attenuation or amplification, respectively. The corresponding attenuation factor (α) can be formulated as [7]:

$$\alpha = \frac{n_c \Xi_u^2}{9 v_s^3 k_B T \rho} \frac{\omega^2 \tau_R \left(1 - \frac{v_d}{v_s}\right)}{\left[1 + \left(1 - \frac{v_d}{v_s}\right)^2 \omega^2 \tau_R^2\right]} \quad (1),$$

where, n_c = density of electrons, Ξ_u = deformation potential constant, τ_R = intervalley relaxation time, v_s = acoustic velocity, v_d = electron drift velocity and other symbols have their usual meanings. Indicatively, negative attenuation (i.e. amplification) occurs when $v_d > v_s$ in Eq. (1). Such criteria can be achieved through application of a DC electric field (E_{dc}) that is strong enough to launch electrons 'faster' than the travelling acoustic wave. The resulting amplification is more pronounced in Ge, compared to any other semiconductor, since it simultaneously provides high electron mobility ($\mu_n \approx 3900\ cm^2/Vs$) and slow acoustic wave velocity ($v_d \approx 2000 - 5000\ m/s$) ; thus requiring lower E_{dc} values to achieve sufficient drift velocity ($v_d = \mu_n E_{dc}$) for acoustoelectric amplification. Figure 1 shows the amplification factor (i.e. -α), over different DC electric fields applied along a (100)-oriented Ge waveguide with a 2μm×200μm cross-sectional dimension, operating in A_0 and S_0 Lamb-wave modes. The maximum acoustoelectric amplification occurs for a DC electric field of ~44 V/mm and ~46 V/mm for A_0 and S_0 Lamb waves, respectively.

III. AlN-on-Ge Lamb Wave Delay Lines

To realize the acoustoelectric physics, unidirectional excitation of acoustic wave is fundamental in assuring traveling nature of the propagating wave. In this work, the travelling Lamb waves are excited using a 200 nm AlN piezoelectric film with single-phase unidirectional transducers (SPUDT) that ensure excitation / reception of traveling wave in forward direction and suppression of backward reflections (Figure 2). The resulting AlN-on-Ge Lamb wave delay line is used for exploration of the acoustoelectric amplification in Ge. Figure 3 demonstrates the COMSOL-simulated transmission response (i.e. $|S_{21}|$) of the delay line in A_0 and S_0 modes for different number of SPUDT cells, assuming the materials to be lossless and considering impedance-matched terminations.

IV. Fabrication Process

AlN-on-Ge Lamb wave delay lines are fabricated using a process flow shown in Figure 4. A 2μm-thick epitaxial Ge is grown on a sacrificial silicon dioxide (SiO_2)-on-silicon (Si) substrate. This is followed by sputtering of a 200 nm AlN film sandwiched between 100 nm molybdenum (Mo) layers. Prior to deposition of the Mo/AlN/Mo stack, a 20 nm AlN layer is sputtered on Ge to electrically isolate the RF signals applied to the piezoelectric transducers from the DC electric field in Ge. This is followed by patterning of SPUDT ports in top Mo, and opening of access windows to bottom Mo, to apply / sense RF signals at the two ports. Furthermore, the piezoelectric stack and AlN seed layer are patterned to create electrical access to Ge waveguide. Next, trenches are etched over the Mo, AlN, and Ge layers in the stack to define the 800μm×200μm lateral geometry of the delay line. Finally, the device is released using holes from top in hydrofluoric acid (HF) by etching sacrificial SiO_2. Figure 5 demonstrates the cross-sectional SEM of the Lamb-wave delay line showing the details of the stack, prior to release. Figure 6 demonstrates the SEM image of the fabricated AlN-on-Ge Lamb wave delay line.

V. Device Characterization

The frequency response of the delay lines is measured using Keysight N5222A Vector Network Analyzer. The electrical signals are excited / sensed at the two ports through the use of RF baluns to enhance the electromechanical transduction efficiency. The DC bias is applied along the Ge waveguide using a Keysight E36105A power supply.

Figure 7 demonstrates the measured transmission response of the delay line in A_0 (at 75 MHz) and S_0 (at 250 MHz) modes, for different acoustoelectric DC bias voltages. Large acoustoelectric amplification of ~6 dB and ~7 dB are achieved for A_0 and S_0 modes through the application of 35V and 42V, respectively. Figure 8 shows the non-reciprocal transmission ratio (i.e. NTR = $|S_{21}|/|S_{12}|$) for the delay line operating in the S_0 mode, when a 42V acoustoelectric DC bias voltage is applied. While the acoustoelectric DC bias amplifies the acoustic wave in forward direction, it induces excessive attenuation in reverse direction. A large NTR of ~10dB is achieved over a 50MHz bandwidth, which corresponds to 10% of the center frequency.

VI. Conclusion

This paper reports, for the first time, on the use of acoustoelectric amplification in single crystal Ge for realization of non-reciprocal RF delay lines. This amplification is enabled by the deformation potential scattering physics that couple acoustic waves to electronic band structures in Ge. Analytical formulation is presented showing the large amplification factors for A_0 and S_0 Lamb waves, when a sufficiently large DC polarization field is applied in the propagation direction. AlN-on-Ge delay line prototypes are designed and implemented operating at 75 MHz and 250 MHZ, showing an amplification of ~6 dB and ~10 dB with the application of 43V and 50V DC voltages, respectively. A non-reciprocal transmission ratio in excess of ~20 dB is measured for the S_0 wave over a 14.9 MHz bandwidth (i.e. 6.9% of the center frequency), highlighting the potential of Ge-based delay lines for realization of non-reciprocal spectral processors to enable integrated full-duplex RF front-end modules.

Acknowledgment

This work is supported by the NSF grant ECCS 1752206.

References

[1] Estep, N.A., Sounas, D.L. and Alù, A., 2016. Magnetless microwave circulators based on spatiotemporally modulated rings of coupled resonators. IEEE Transactions on Microwave Theory and Techniques, 64(2), pp.502-518.

[2] Reiskarimian, N. and Krishnaswamy, H., 2016. Magnetic-free non-reciprocity based on staggered commutation. Nature comm., 7, p.11217.

[3] Ghatge, M., Walters, G., Nishida, T. and Tabrizian, R., 2019. A non-reciprocal filter using asymmetrically transduced micro-acoustic resonators. IEEE Electron Device Letters, 40(5), pp.800-803.

[4] Zhu, H. and Rais-Zadeh, M., 2017. Non-reciprocal acoustic transmission in a GaN delay line using the acoustoelectric effect. IEEE Electron Device Letters, 38(6), pp.802-805.

[5] M. Rotter, A. Wixforth, W. Ruile, D. Bernklau, and H. Riechert, "Giant acoustoelectric effect in GaAs/LiNbO3 hybrids," APL, vol. 73, pp. 2128-2130.

[6] Bhaskar, U.K., Bhave, S.A. and Weinstein, D., 2018. Silicon acoustoelectronics with thin film lithium niobate. Journal of Physics D: Applied Physics, 52(5), p.05LT01.

[7] M. Pomerantz, "Ultrasonic loss and gain mechanisms in semiconductors," Proceedings of the IEEE, vol. 53, pp. 1438-1451, 1965.

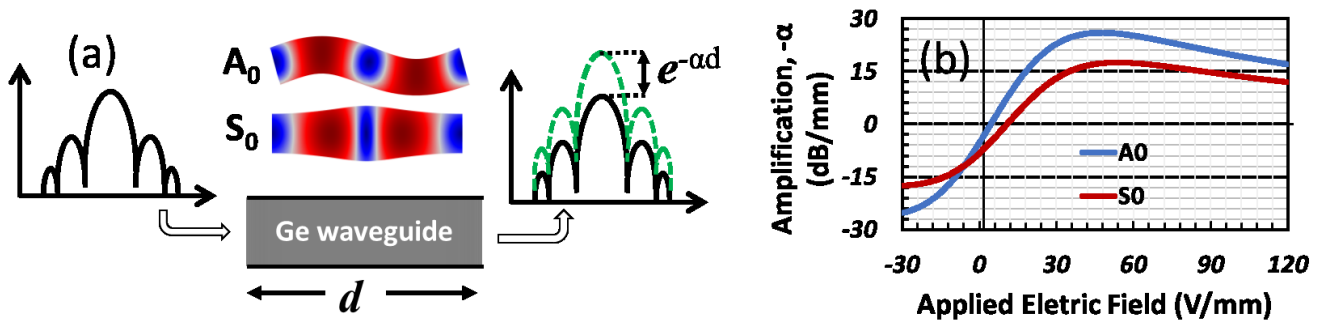

Figure 1: (a) Spectral representation of acoustoelectric amplification ($\alpha<0$) along with displacement profiles of anti-symmetric (A_0) and symmetric (S_0) lamb wave modes in Germanium (Ge) (b) Estimation of acoustoelectric amplification in Ge at different applied electric fields for A_0 and S_0 lamb wave modes having phase velocity of 1790 m/s and 4315 m/s respectively.

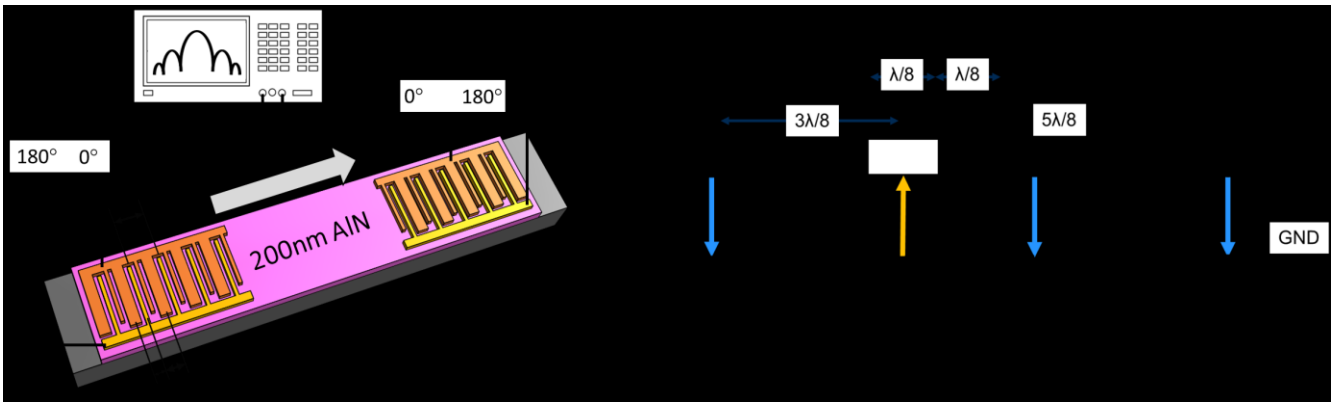

Figure 2: (a) Schematic demonstration of the AlN-on-Ge delay line and measurement setup for obtaining frequency response. The delay line comprises of two set of single-phase unidirectional transducers (SPUDT). The input and output SPUDTs are connected to Vector Network Analyzer (VNA) through a RF balun for out of phase voltage actuation and sensing respectively. (b) Electric field distribution inside piezoelectric layer upon application of out of phase voltages in single phase unidirectional transducers (SPUDT) using RF Balun. The blue and yellow arrows represent the direction of electric fields when 0° and 180° phase shifted voltages are applied in corresponding electrodes. The dashed line at the bottom indicates grounded electrode. Fourier analysis of SPUDTs show that the generated wave has phase angle of 90° which interferes constructively with reflectors situated at 5λ/8 and destructively with reflectors situated at 3λ/8 which validate the unidirectional nature of the SPUDTs.

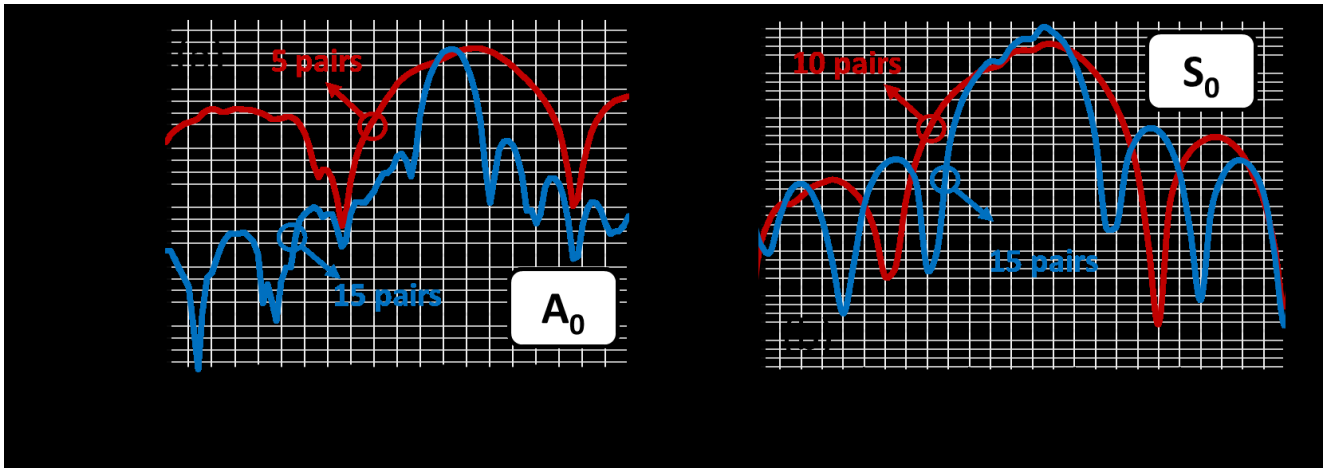

Figure 3: COMSOL-simulated transmission response (i.e. $|S_{21}|$) of the 800μm-long delay line with different SPUDT cell numbers for (a) A_0 and (b) S_0 Lamb waves. The sinc-shaped transfer function for the A_0 and S_0 modes are located at 72 MHz (for 5 and 15 pairs of SPUDT cells) and 267 MHz (for 10 and 15 pairs of SPUDT cells), respectively. The slanted / non-symmetric pass-band of the S_0 delay line is attributed to the phase velocity dispersion. In the simulations perfectly matched mechanical boundaries, at the two terminations of delay lines, along with matched-impedance electrical termination are used.

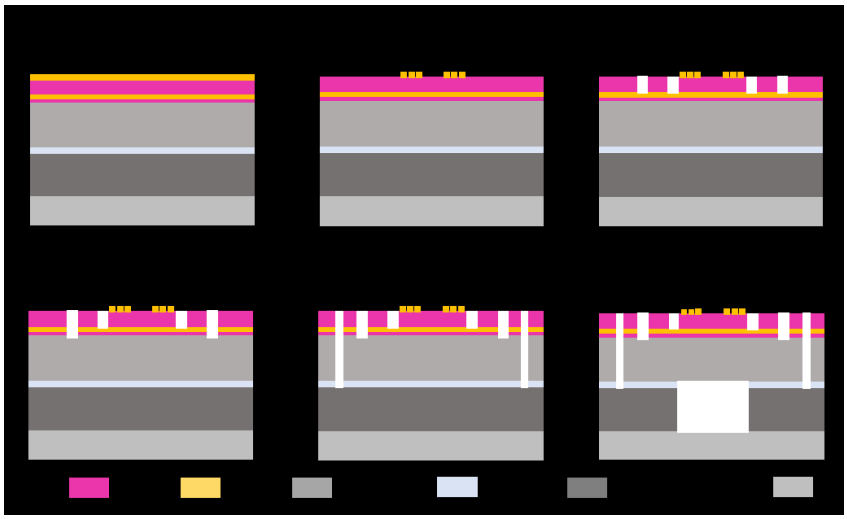

Figure 4: Fabrication process flow of for implementation of AlN-on-Ge delay lines. Top Mo SPUDTs serve as RF signal pads and bottom Mo serve as GND pad. The DC bias is applied by accessing Ge. The DC and RF fields are isolated through a 20nm AlN layer.

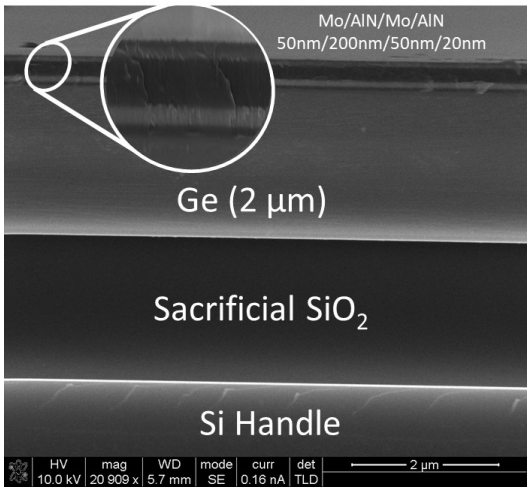

Figure 5: Cross-sectional SEM image of the fabricated AlN-on-Ge delay line: stack of Mo/AlN/Mo/AlN-seed/Ge/Si-seed/SiO_2/Si Handle. The inset shows the details of the piezoelectric transducer stack.

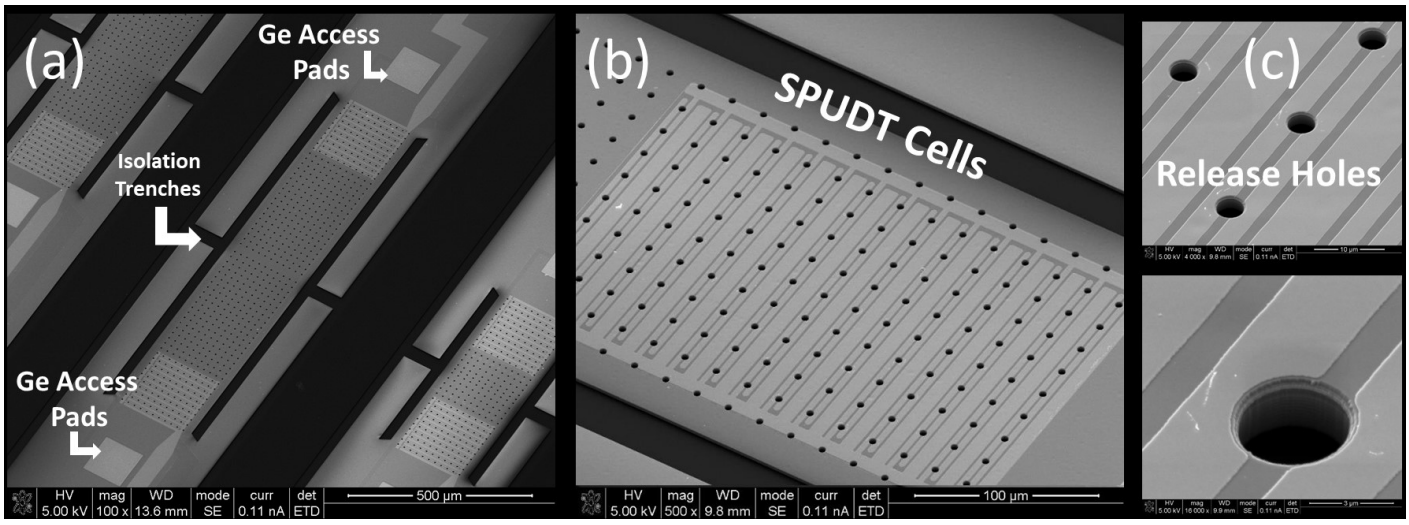

Figure 6: The SEM images of the delay line highlighting (a) the lateral geometry of defined by isolation trenches, the input / output SPUDT ports, and the Ge access pads to apply acoustoelectric DC bias across the waveguide; (b) the zoomed-in image of SPUDT port composed of 15 cells; (c) the zoomed-in image of the periodic holes etched through the stack to enable release of the delay line by etching sacrificial SiO_2 in HF.

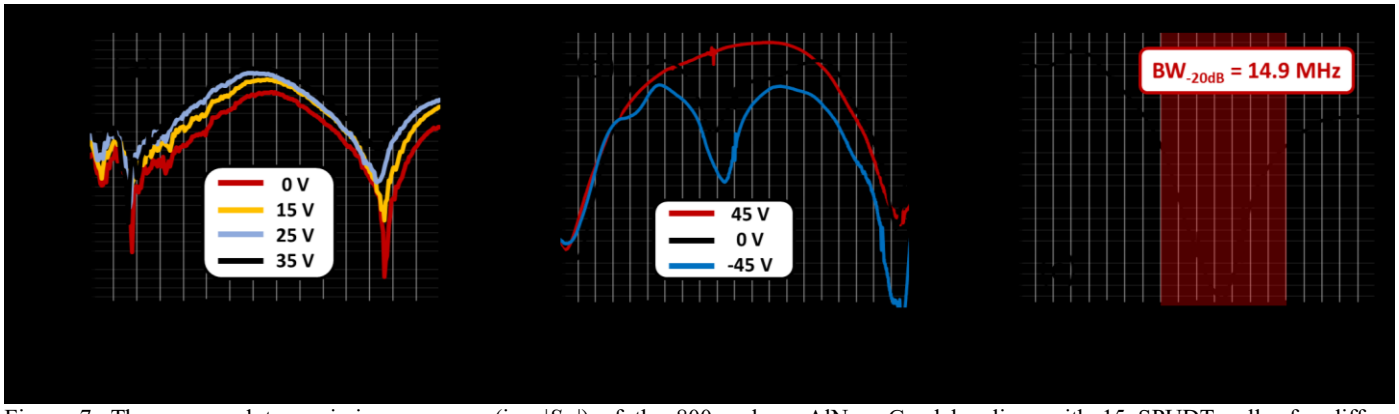

Figure 7: The measured transmission response (i.e. $|S_{21}|$) of the 800µm-long AlN-on-Ge delay line, with 15 SPUDT cells, for different acoustoelectric DC bias voltages when operating in (a) A_0 mode and (b) S_0 mode. Amplification levels of ~6 dB (with 35V of DC bias) and ~7 dB (with 45V of DC bias) are measured for A_0 and S_0 modes, respectively. (c) The measured non-reciprocal transmission ratio (i.e. NTR = $|S_{21}|/|S_{12}|$) for the S0 mode, when a 45V DC bias is applied across the Ge waveguide. While the wave is amplified in the forward direction (corresponding to S_{21}), it gets attenuated in reverse direction (corresponding to S_{12}). A 14.9 MHz of >20dB NTR corresponds to a fraction bandwidth of 6.7%.